Available online at www.sciencedirect.com
SCIENCE DIRECT®
Computer methods in applied mechanics and engineering
Comput. Methods Appl. Mech. Engrg. xxx (2004) xxx–xxx
www.elsevier.com/locate/cma

Stabilized finite elements applied to elastoplasticity: I. Mixed displacement–pressure formulation

Stéphane Commend, Andrzej Truty [1], Thomas Zimmermann *

Laboratory of Structural and Continuum Mechanics, Department of Civil Engineering, ENAC, Swiss Federal Institute of Technology, CH-1015 Lausanne, EPFL, Switzerland

Received 5 November 2001; received in revised form 17 October 2003; accepted 7 January 2004

Abstract

A stabilized, mixed, displacement–pressure (u–p), finite element formulation for elasto-plastic solid media is developed in this paper. In particular it applies to low order finite elements with equal interpolation order for both displacement and pressure fields. The approach successfully eliminates the effect of volumetric locking for elastic nearly incompressible media and the elasto-plastic media exhibiting incompressible or dilatant plastic flow. The performance of the proposed formulation is compared with the stabilized formulation based on pressure Laplacian. It is shown that the proposed stabilized formulation also supports mixing different elements.

IDT: 28; 40; 65; 78
Keywords: Stabilized finite elements; Elastoplasticity; Mixing different elements

1. Introduction

Standard displacement-based finite element methods are known to behave poorly for nearly incompressible or dilatant/contractant elasto-plastic media, exhibiting volumetric locking effect and failing to correctly reproduce ultimate loads in limit state analyses. Well-known finite elements which overcome these difficulties include the family of $\overline{\mathbf{B}}$ elements [11], enhanced-assumed strain (EAS) elements [16] or high-order mixed displacement–pressure formulations [21]. In this paper we consider an alternative approach based on the stabilization of a mixed displacement–pressure low-order finite element formulation.

Stabilized methods have been applied with great success over the last twenty years in the field of computational fluid dynamics [2,8,10,12]. In particular, they have proven to be efficient in the treatment of advection-dominated advection–diffusion flows. Another advantage of such methods is their ability to overcome difficulties associated with mixed formulations (like inappropriate combination of interpolation

* Corresponding author.
E-mail address: thomas.zimmermann@epfl.ch (T. Zimmermann).
[1] Currently at Department of Environmental Engineering, Cracow University of Technology, ul. Warszawska 24, 31-155 Kraków, Poland.

0045-7825/$ - see front matter © 2004 Published by Elsevier B.V.
doi:10.1016/j.cma.2004.01.007

Nomenclature

Ω	a given body without its boundary
$\Gamma = \Gamma_{g_i} \cup \Gamma_{h_i}$	Ω's boundary
E	Young's modulus
ν	Poisson's ratio
K	elastic bulk modulus
μ	shear modulus
σ_{ij}	stress tensor component
δ_{ij}	Kronecker's symbol
$\boldsymbol{\sigma}$	stress vector with components (in 3D): $\boldsymbol{\sigma} = \{\sigma_{11}, \sigma_{22}, \sigma_{12}, \sigma_{33}, \sigma_{13}, \sigma_{23}\}^{\mathrm{T}}$
$\boldsymbol{\varepsilon}$	total strain vector with components (in 3D): $\boldsymbol{\varepsilon} = \{\varepsilon_{11}, \varepsilon_{22}, \gamma_{12}, \varepsilon_{33}, \gamma_{13}, \gamma_{23}\}^{\mathrm{T}}$
$\mathbf{1}$	Kronecker's vector (in 3D): $= \{1, 1, 0, 1, 0, 0\}^{\mathrm{T}}$
ε_{ij}	total strain tensor component
$\varepsilon_{ij}^{\mathrm{p}}$	total plastic strain tensor component
$\boldsymbol{\varepsilon}^{\mathrm{p}}$	plastic strain vector with components ordered as above
$f(\boldsymbol{\sigma})$	yield function
$g(\boldsymbol{\sigma})$	plastic potential
$\dot{\gamma}$	plastic multiplier
$\mathbf{r}(\boldsymbol{\sigma})$	plastic flow vector
u_i	displacement component
$\mathbf{u}$	displacement vector
p	mean pressure
w_i	component of displacement weighting function
$\mathbf{w}$	vector of displacement weighting functions
q	pressure weighting function
D_{ijkl}	component of elastic constitutive tensor
$\overline{D}_{ijkl}$	deviatoric projection of the elastic constitutive tensor
$\overline{\mathbf{D}}^{uu}, \overline{\mathbf{D}}^{up}, \overline{\mathbf{D}}^{pu}, \overline{\mathbf{D}}^{pp}$	elastoplastic tangent constitutive submatrices
$\overline{\mathbf{K}}^{uu}, \overline{\mathbf{K}}^{up}, \overline{\mathbf{K}}^{pu}, \overline{\mathbf{K}}^{pp}$	stiffness submatrices
$\mathbf{F}_u, \mathbf{F}_p$	right-hand side subvectors
$\boldsymbol{\tau}$	stabilization factor matrix
α^e	stabilization scalar factor
h^e	characteristic length of an element
N_i	displacement shape function
$\mathbf{N}$	vector of displacement shape functions
$\widetilde{N}_i$	pressure shape function
$\widetilde{\mathbf{N}}$	vector of pressure shape functions
$(\cdot)^i$	quantity $(\cdot)$ at iteration i
$(\cdot)_n$	quantity $(\cdot)$ at step t_n
$\Delta(\cdot)$	increment of quantity $(\cdot)$
$\Delta(\cdot)_{n+1}$	increment of quantity $(\cdot)$ between steps t_n and t_{n+1}
$(\cdot)_{,i}$	indicates derivation of $(\cdot)$ with respect to x_i

$\vec{\nabla}(\cdot)$	gradient of quantity $(\cdot)$
$\lvert(\cdot)\rvert$	absolute value of $(\cdot)$
$(\cdot)^e$	quantity $(\cdot)$ at an element node
$(\cdot)^h$	quantity $(\cdot)$ approximated inside an element

fields), thus making it possible to use low-order finite elements, which are convenient from the implementational point of view, easy to generate, and cheap in large-scale computations.

We apply here the same stabilization framework in the context of elasto-plastic solids [5]. Three different approaches to stabilization are scrutinized: a form which results from modifications to the Galerkin/least-squares method [10,12], the Laplacian pressure operator scheme [4,15] and the finite increment calculus approach [13,14]. The first two schemes are discussed in this paper, while the third, which provides a tentative justification as well as the possibility of introducing a directional character into the formulation, will be addressed separately in a companion paper [6].

To our knowledge the stabilized formulation is the only one which allows the use of low-order interpolation functions for both displacement and the pressure field, eliminates volumetric locking effect and is able to circumvent numerical instabilities in the pressure field. The extension of such stabilized formulations to two-phase problems also overcomes pore-pressure oscillations when the critical time step condition is violated in consolidation problems [18,19] and accommodates the mixture of different elements within the same mesh (for instance linear triangles and bilinear quadrilaterals), while the discussion is limited in this paper to nearly incompressible media, the same approach is shown to also work for dilatant media in [6].

The rest of the paper is structured as follows: in Section 1 a nonlinear mixed displacement–pressure formulation for elasto-plasticity is derived. Then in Section 2 two different stabilization techniques are discussed, as well as the selection of optimal stabilization factors. Section 3 includes two benchmark problems which validate the approach, namely, a nearly incompressible elasticity analogy with the driven cavity Stokes flow problem, and an elasto-plastic thick cylinder loaded by an internal pressure. Finally, conclusions are drawn in Section 4.

2. Governing equations

2.1. Constitutive modelling: mixed formulation of perfect plasticity

We adopt the following volumetric–deviatoric split of the constitutive equation, expressed in the matrix notation as follows (see e.g. [21]):

$$\dot{\boldsymbol{\sigma}} = \overline{\mathbf{D}}[\dot{\boldsymbol{\varepsilon}} - \dot{\boldsymbol{\varepsilon}}^{\mathrm{p}}] + \mathbf{1}\dot{p}, \tag{1}$$

$$\mathbf{1}^{\mathrm{T}}(\dot{\boldsymbol{\varepsilon}} - \dot{\boldsymbol{\varepsilon}}^{\mathrm{p}}) - \dot{p}/K = 0. \tag{2}$$

The deviatoric projection $\overline{\mathbf{D}}$ of the elastic constitutive matrix $\mathbf{D}$ is defined as:

$$\overline{\mathbf{D}} = \mathbf{D}\left(\mathbf{I} - \tfrac{1}{3}\mathbf{1}\mathbf{1}^{\mathrm{T}}\right), \tag{3}$$

where $\mathbf{I}$ is the identity matrix and $\mathbf{1}$ the vectorial representation of Kronecker's delta δ_{ij}. Additive decomposition of the elastic and plastic strain rates is used:

$$\dot{\boldsymbol{\varepsilon}} = \dot{\boldsymbol{\varepsilon}}^{e} + \dot{\boldsymbol{\varepsilon}}^{\mathrm{p}}. \tag{4}$$

Additional ingredients of the standard elasto-plasticity formulation include a yield function:

$$f(\boldsymbol{\sigma}) = 0, \tag{5}$$

a flow rule:

$$\dot{\boldsymbol{\varepsilon}}^{\mathrm{p}} = \dot{\gamma}\frac{\partial g}{\partial \boldsymbol{\sigma}} = \dot{\gamma}\mathbf{r}(\boldsymbol{\sigma}), \tag{6}$$

where $\dot{\gamma}$ is the scalar plastic multiplier and g is the plastic potential; Finally consistency implies:

$$\dot{\gamma} f(\boldsymbol{\sigma}) = 0. \tag{7}$$

2.2. Strong form

Consider a body Ω, its boundary $\partial\Omega = \Gamma = \overline{\Gamma_{g_i} \cup \Gamma_{h_i}}$ with $\Gamma_{g_i} \cap \Gamma_{h_i} = \emptyset$, with $i = 1, \ldots, n_{\mathrm{sd}}$, where n_{sd} stands for the number of spatial dimensions. Given $f_i : \Omega \to \mathbb{R}$, $g_i : \Gamma_{g_i} \to \mathbb{R}$ and $h_i : \Gamma_{h_i} \to \mathbb{R}$, find $u_i : \overline{\Omega} \to \mathbb{R}$ and $p : \overline{\Omega} \to \mathbb{R}$ such that:

$$\sigma_{ij,j} + f_i = 0 \quad \text{equilibrium in } \Omega, \tag{8}$$

$$\varepsilon_{ii} - \varepsilon^{\mathrm{p}}_{ii} - \frac{p}{K} = 0 \quad \text{volumetric constitutive equation in } \Omega, \tag{9}$$

$$u_i = g_i \quad \text{Dirichlet boundary condition on } \Gamma_{g_i}, \tag{10}$$

$$\sigma_{ij} n_j = h_i \quad \text{Neumann boundary condition on } \Gamma_{h_i}, \tag{11}$$

where the rate of $\sigma_{ij}(\mathbf{u}, p)$ is expressed by Eq. (1) and $K = \frac{E}{3(1-2\nu)}$ is the elastic bulk modulus.

2.3. Discretized weak form

A weak formulation of the mixed problem can easily be derived (see e.g. [11]).
Let:

$$\mathscr{S}_i = \{u_i \in H^1(\Omega) | u_i = g_i \text{ on } \Gamma_{g_i}\}, \tag{12}$$

$$\mathscr{V}_i = \{w_i \in H^1(\Omega) | w_i = 0 \text{ on } \Gamma_{g_i}\}, \tag{13}$$

$$\mathscr{P} = \{p \in L^2(\Omega)\}, \tag{14}$$

where H^1 and L^2 are appropriate Hilbert spaces. $\mathscr{S}_i$ represents the trial solution space, $\mathscr{V}_i$ the weighting function space and $\mathscr{P}$ the pressure space. Introducing the finite-dimensional subspaces $\mathscr{S}_i^h \subset \mathscr{S}_i$, $\mathscr{V}_i^h \subset \mathscr{V}_i$ and $\mathscr{P}^h \subset \mathscr{P}$, we can express the discretized Galerkin form of the problem as: given f_i, g_i and h_i as before, we wish to find $u_i^h = (v_i^h + g_i^h) \in \mathscr{S}_i^h$ (with $v_i^h \in \mathscr{V}_i^h$) and $p^h \in \mathscr{P}^h$ such that, for all $w_i^h \in \mathscr{V}_i^h$ and $q^h \in \mathscr{P}^h$, the following equations hold (in vector notations):

$$\int_\Omega \boldsymbol{\varepsilon}(\mathbf{w}^h)^{\mathrm{T}} \boldsymbol{\sigma}(\mathbf{u}^h, p^h)\,\mathrm{d}\Omega = \int_{\Gamma_h} (\mathbf{w}^h)^{\mathrm{T}} \mathbf{h}\,\mathrm{d}\Gamma + \int_\Omega (\mathbf{w}^h)^{\mathrm{T}} \mathbf{f}\,\mathrm{d}\Omega, \tag{15}$$

$$\int_\Omega q^h \mathbf{1}^{\mathrm{T}} (\boldsymbol{\varepsilon}(\mathbf{u}^h) - \boldsymbol{\varepsilon}^{\mathrm{p}}(\mathbf{u}^h, p^h))\,\mathrm{d}\Omega - \int_\Omega q^h \frac{p^h}{K}\,\mathrm{d}\Omega = 0. \tag{16}$$

2.4. Linearization

As we deal with elasto-plasticity, a residual-driven iterative scheme is needed. Assuming that the two preceding equations must be satisfied at step $(n+1)$ we have:

$$\int_{\Omega} \mathbf{B}^{\mathrm{T}} \boldsymbol{\sigma}_{n+1} \, \mathrm{d}\Omega = \mathbf{F}_{\mathrm{ext},n+1}, \tag{17}$$

$$\int_{\Omega} \widetilde{\mathbf{N}}^{\mathrm{T}} \mathbf{1}^{\mathrm{T}} (\boldsymbol{\varepsilon}_{n+1} - \boldsymbol{\varepsilon}^{\mathrm{p}}_{n+1}) \, \mathrm{d}\Omega - \int_{\Omega} \widetilde{\mathbf{N}}^{\mathrm{T}} \frac{p_{n+1}}{K} \, \mathrm{d}\Omega = 0, \tag{18}$$

where pressure shape functions are denoted by $\widetilde{\mathbf{N}}$ and $\mathbf{B}$ is the standard strain–displacement operator including spatial derivatives of displacement shape functions.

2.4.1. Equilibrium equation

Applying a full implicit integration scheme for plastic strains the constitutive equation can be expressed in its integrated form, at step $(n+1)$, as:

$$\boldsymbol{\sigma}_{n+1} = \overline{\mathbf{D}}[\boldsymbol{\varepsilon}_{n+1} - \boldsymbol{\varepsilon}^{\mathrm{p}}_{n+1}] + \mathbf{1} p_{n+1}, \tag{19}$$

where

$$\boldsymbol{\varepsilon}^{\mathrm{p}}_{n+1} = \boldsymbol{\varepsilon}^{\mathrm{p}}_{n} + \Delta\gamma_{n+1} \mathbf{r}(\boldsymbol{\sigma}_{n+1}). \tag{20}$$

Hence the linearized equation (17) takes the form

$$\int_{\Omega} \mathbf{B}^{\mathrm{T}} \Delta\boldsymbol{\sigma} \, \mathrm{d}\Omega = \mathbf{F}_{\mathrm{ext},n+1} - \int_{\Omega} \mathbf{B}^{\mathrm{T}} \boldsymbol{\sigma}^{i}_{n+1} \, \mathrm{d}\Omega, \tag{21}$$

and the stress correction is expressed as follows:

$$\Delta\boldsymbol{\sigma} = \overline{\mathbf{D}} \left(\Delta\boldsymbol{\varepsilon} - \Delta\gamma \mathbf{r}_{n+1} - \Delta\gamma_{n+1} \frac{\partial \mathbf{r}_{n+1}}{\partial \boldsymbol{\sigma}} \Delta\boldsymbol{\sigma} \right) + \mathbf{1} \Delta p. \tag{22}$$

Rearranging the terms we get:

$$\Delta\boldsymbol{\sigma} = \overline{\mathbf{D}}^{*} (\Delta\varepsilon - \Delta\gamma \mathbf{r}) + \overline{\mathbf{C}}^{*} \Delta p, \tag{23}$$

with auxiliary matrices $\overline{\mathbf{D}}^{*}$, $\overline{\mathbf{C}}^{*}$ and $\mathbf{A}$:

$$\overline{\mathbf{D}}^{*} = \mathbf{A}^{-1} \overline{\mathbf{D}}, \tag{24}$$

$$\overline{\mathbf{C}}^{*} = \mathbf{A}^{-1} \mathbf{1}, \tag{25}$$

$$\mathbf{A} = \left(\mathbf{I} + \Delta\gamma_{n+1} \frac{\partial \mathbf{r}_{n+1}}{\partial \boldsymbol{\sigma}} \right). \tag{26}$$

The increment of plastic multiplier $\Delta\gamma$ appearing in Eq. (23) can be expressed through total strain and mean pressure increments via consistency condition $\dot{f} = 0$ (equivalent to the expression $(\frac{\partial f}{\partial \boldsymbol{\sigma}_{n+1}})^{\mathrm{T}} \Delta\boldsymbol{\sigma} = 0$), which yields

$$\Delta\gamma = \frac{\left(\frac{\partial f}{\partial \boldsymbol{\sigma}_{n+1}} \right)^{\mathrm{T}} \overline{\mathbf{D}}^{*} \Delta\varepsilon + \left(\frac{\partial f}{\partial \boldsymbol{\sigma}_{n+1}} \right)^{\mathrm{T}} \overline{\mathbf{C}}^{*} \Delta p}{\left(\frac{\partial f}{\partial \boldsymbol{\sigma}_{n+1}} \right)^{\mathrm{T}} \overline{\mathbf{D}}^{*} \mathbf{r}}. \tag{27}$$

Introducing $\Delta\gamma$ into Eq. (23) we get the final form of the stress correction $\Delta\sigma$:

$$\Delta\boldsymbol{\sigma} = \left(\overline{\mathbf{D}}^{*} - \frac{\overline{\mathbf{D}}^{*}\mathbf{r}\left(\frac{\partial f}{\partial \boldsymbol{\sigma}_{n+1}}\right)^{\mathrm{T}}\overline{\mathbf{D}}^{*}}{\left(\frac{\partial f}{\partial \boldsymbol{\sigma}_{n+1}}\right)^{\mathrm{T}}\overline{\mathbf{D}}^{*}\mathbf{r}}\right)\Delta\varepsilon + \left(\overline{\mathbf{C}}^{*} - \frac{\overline{\mathbf{D}}^{*}\mathbf{r}\left(\frac{\partial f}{\partial \boldsymbol{\sigma}_{n+1}}\right)^{\mathrm{T}}\overline{\mathbf{C}}^{*}}{\left(\frac{\partial f}{\partial \boldsymbol{\sigma}_{n+1}}\right)^{\mathrm{T}}\overline{\mathbf{D}}^{*}\mathbf{r}}\right)\Delta p, \tag{28}$$

which we can express in compact form as:

$$\Delta\sigma = \overline{\mathbf{D}}^{uu}\Delta\varepsilon + \overline{\mathbf{D}}^{up}\Delta p, \tag{29}$$

or:

$$\Delta\sigma = \overline{\mathbf{D}}^{uu}\mathbf{B}\Delta\mathbf{u} + \overline{\mathbf{D}}^{up}\widetilde{\mathbf{N}}\Delta\mathbf{p}. \tag{30}$$

Hence the final form of the linearized Eq. (21) takes the following form, at step $(n+1)$ and iteration $(i+1)$:

$$\int_{\Omega}\mathbf{B}^{\mathrm{T}}\overline{\mathbf{D}}^{uu}\mathbf{B}\Delta\mathbf{u}\,\mathrm{d}\Omega + \int_{\Omega}\mathbf{B}^{\mathrm{T}}\overline{\mathbf{D}}^{up}\widetilde{\mathbf{N}}\Delta\mathbf{p}\,\mathrm{d}\Omega = \mathbf{F}_{\mathrm{ext},n+1} - \int_{\Omega}\mathbf{B}^{\mathrm{T}}\boldsymbol{\sigma}^{i}_{n+1}\,\mathrm{d}\Omega. \tag{31}$$

During the iterative process, the accumulated values of the displacement and the pressure are updated as follows:

$$\Delta\mathbf{u}^{i+1}_{n+1} = \Delta\mathbf{u}^{i}_{n+1} + \Delta\mathbf{u}, \tag{32}$$

$$\Delta\mathbf{p}^{i+1}_{n+1} = \Delta\mathbf{p}^{i}_{n+1} + \Delta\mathbf{p}, \tag{33}$$

Remark 1. $\Delta p^{h,i+1}_{n+1}$ can be viewed as the mean pressure of the stress increment $\Delta\boldsymbol{\sigma}^{i+1}_{n+1}$ if and only if the step is converged. During the iterations, it does not always coincide with the hydrostatic part of the hydro static-deviatoric split of the stress increment tensor.

2.4.2. Continuity equation

The linearized form of the pressure constitutive equation is expressed in the form:

$$\int_{\Omega}\widetilde{\mathbf{N}}^{\mathrm{T}}\mathbf{1}^{\mathrm{T}}\left(\Delta\boldsymbol{\varepsilon} - \Delta\gamma\mathbf{r} - \Delta\gamma_{n+1}\frac{\partial\mathbf{r}}{\partial\boldsymbol{\sigma}}\Delta\boldsymbol{\sigma}\right)\mathrm{d}\Omega - \int_{\Omega}\widetilde{\mathbf{N}}^{\mathrm{T}}\frac{\Delta p}{K}\,\mathrm{d}\Omega = \mathbf{R}^{i}_{\theta,n+1}, \tag{34}$$

with the residual term $\mathbf{R}^{i}_{\theta,n+1}$ expressed as follows:

$$\mathbf{R}^{i}_{\theta,n+1} = -\int_{\Omega}\widetilde{\mathbf{N}}^{\mathrm{T}}\left(\mathbf{1}^{\mathrm{T}}(\boldsymbol{\varepsilon}^{i}_{n+1} - \boldsymbol{\varepsilon}^{p,i}_{n+1}) - \frac{p^{i}_{n+1}}{K}\right)\mathrm{d}\Omega. \tag{35}$$

If we restrict our consideration to the Drucker–Prager model then the term $\Delta\gamma_{n+1}\mathbf{1}^{\mathrm{T}}\frac{\partial\mathbf{r}}{\partial\boldsymbol{\sigma}}\Delta\boldsymbol{\sigma}$ disappears.

$$\int_{\Omega}\widetilde{\mathbf{N}}^{\mathrm{T}}\left(\mathbf{1}^{\mathrm{T}} - \frac{\mathbf{1}^{\mathrm{T}}\mathbf{r}\left(\frac{\partial f}{\partial \boldsymbol{\sigma}_{n+1}}\right)^{\mathrm{T}}\overline{\mathbf{D}}^{*}}{\left(\frac{\partial f}{\partial \boldsymbol{\sigma}_{n+1}}\right)^{\mathrm{T}}\overline{\mathbf{D}}^{*}\mathbf{r}}\right)\Delta\boldsymbol{\varepsilon}\,\mathrm{d}\Omega - \int_{\Omega}\widetilde{\mathbf{N}}^{\mathrm{T}}\left(\frac{1}{K} + \frac{\mathbf{1}^{\mathrm{T}}\mathbf{r}\left(\frac{\partial f}{\partial \boldsymbol{\sigma}_{n+1}}\right)^{\mathrm{T}}\overline{\mathbf{C}}^{*}}{\left(\frac{\partial f}{\partial \boldsymbol{\sigma}_{n+1}}\right)^{\mathrm{T}}\overline{\mathbf{D}}^{*}\mathbf{r}}\right)\widetilde{\mathbf{N}}\Delta\mathbf{p}\,\mathrm{d}\Omega = \mathbf{R}^{i}_{\theta,n+1}, \tag{36}$$

or in compact form:

$$\int_{\Omega}\widetilde{\mathbf{N}}^{\mathrm{T}}\overline{\mathbf{D}}^{pu}\mathbf{B}\Delta\mathbf{u}\,\mathrm{d}\Omega + \int_{\Omega}\widetilde{\mathbf{N}}^{\mathrm{T}}\overline{\mathbf{D}}^{pp}\widetilde{\mathbf{N}}\Delta\mathbf{p}\,\mathrm{d}\Omega = \mathbf{R}^{i}_{\theta,n+1}, \tag{37}$$

Remark 2. In the case of J2-Plasticity (von Mises), $\overline{\mathbf{D}}^{pu}$ is reduced to $\mathbf{1}^{\mathrm{T}}$ and $\overline{\mathbf{D}}^{pp}$ reduces to $-\frac{1}{K}$ as $\mathbf{r}$ is orthogonal to $\mathbf{1}$ and therefore $\mathbf{1}^{\mathrm{T}}\mathbf{r} = 0$.

2.5. Matrix form

By grouping Eqs. (31) and (37), we get:

$$\begin{bmatrix} \mathbf{K}_{uu} & \mathbf{K}_{up} \\ \mathbf{K}_{pu} & \mathbf{K}_{pp} \end{bmatrix} \begin{Bmatrix} \Delta\mathbf{u} \\ \Delta\mathbf{p} \end{Bmatrix} = \begin{Bmatrix} \mathbf{F}_u \\ \mathbf{F}_p \end{Bmatrix}, \tag{38}$$

with the left-hand side:

$$\mathbf{K}_{uu} = \int_\Omega \mathbf{B}^{\mathrm{T}} \overline{\mathbf{D}}^{uu} \mathbf{B} \, \mathrm{d}\Omega, \tag{39}$$

$$\mathbf{K}_{up} = \int_\Omega \mathbf{B}^{\mathrm{T}} \overline{\mathbf{D}}^{up} \widetilde{\mathbf{N}} \, \mathrm{d}\Omega, \tag{40}$$

$$\mathbf{K}_{pu} = \int_\Omega \widetilde{\mathbf{N}}^{\mathrm{T}} \overline{\mathbf{D}}^{pu} \mathbf{B} \, \mathrm{d}\Omega, \tag{41}$$

$$\mathbf{K}_{pp} = \int_\Omega \widetilde{\mathbf{N}}^{\mathrm{T}} \overline{\mathbf{D}}^{pp} \widetilde{\mathbf{N}} \, \mathrm{d}\Omega, \tag{42}$$

and the right-hand side:

$$\mathbf{F}_u = \mathbf{F}_{\mathrm{ext},n+1} - \int_\Omega \mathbf{B}^{\mathrm{T}} \boldsymbol{\sigma}^i_{n+1} \, \mathrm{d}\Omega, \tag{43}$$

$$\mathbf{F}_p = \mathbf{R}^i_{\theta,n+1}. \tag{44}$$

The second line of Eq. (38) is then multiplied by -1 in order to achieve positive-definiteness:

$$\begin{bmatrix} \mathbf{K}_{uu} & \mathbf{K}_{up} \\ -\mathbf{K}_{pu} & -\mathbf{K}_{pp} \end{bmatrix} \begin{Bmatrix} \Delta\mathbf{u} \\ \Delta\mathbf{p} \end{Bmatrix} = \begin{Bmatrix} \mathbf{F}_u \\ -\mathbf{F}_p \end{Bmatrix}. \tag{45}$$

3. Stabilization techniques

3.1. Galerkin/least-squares approach

Similarly to what has been done in the computational fluid dynamics framework [8,10,12], we add appropriate terms to the matrix equation (45) in order to enhance its stability. These terms take the form:

$$\sum_{e=1}^{n_{\mathrm{el}}} \int_{\Omega^e} (\mathbf{L}^{\mathrm{T}} \boldsymbol{\sigma}(\mathbf{w}^h, q^h))^{\mathrm{T}} \boldsymbol{\tau} (\mathbf{L}^{\mathrm{T}} \boldsymbol{\sigma}(\mathbf{u}^h, p^h) + \mathbf{f}) \, \mathrm{d}\Omega, \tag{46}$$

where $\boldsymbol{\tau}$ is a stabilization factor matrix, with $\boldsymbol{\tau} = \tau\mathbf{I}$. The nature of τ will be discussed later. The weighting part and the residual part of Eq. (46) will now be addressed separately.

3.2. Towards modified—GLS schemes

In the elasto-plastic case, the weighting part of the stabilization term (Eq. (46)) can be written as:

$$\mathbf{L}^{\mathrm{T}} \boldsymbol{\sigma}(\mathbf{w}^h, q^h) = \mathbf{L}^{\mathrm{T}} (\overline{\mathbf{D}} (\boldsymbol{\varepsilon}(\mathbf{w}^h) - \boldsymbol{\varepsilon}^{\mathrm{p}}(\mathbf{w}^h, q^h)) + \mathbf{1} q^h). \tag{47}$$

As shown in [5], we modify the standard GLS scheme by dropping the plastic contribution, avoiding therefore linearization of the weighting part of the stabilizing terms, and the weighting term $\mathbf{L}^{\mathrm{T}}\sigma(\mathbf{w}^h, q^h)$ is replaced by the $\mathbf{P}(\mathbf{w}^h, q^h)$

$$\mathbf{P}(\mathbf{w}^h, q^h) = \mathbf{L}^{\mathrm{T}}\overline{\mathbf{D}}\mathbf{B}\mathbf{w} + \mathbf{L}^{\mathrm{T}}\mathbf{1}\widetilde{\mathbf{N}}\mathbf{q} \overset{\text{def.}}{=} \mathbf{G}_p^{\mathrm{el}}\mathbf{w} + \mathbf{G}_p^{\mathrm{el}}\mathbf{q}. \tag{48}$$

The two following possible stabilization schemes, GLS-A and GLS-B, which differ in the form of the weighting term $\mathbf{P}(\mathbf{w}^h, q^h)$ are considered:

$$\mathbf{P}^{\text{GLS-A}}(\mathbf{w}^h, q^h) = \mathbf{G}_u^{\mathrm{el}}\mathbf{w} + \mathbf{G}_p^{\mathrm{el}}\mathbf{q}, \tag{49}$$

$$\mathbf{P}^{\text{GLS-B}}(q^h) = \mathbf{G}_p^{\mathrm{el}}\mathbf{q}. \tag{50}$$

Remark 3. The $\mathbf{G}_u^{\mathrm{el}}$ term will vanish for linear triangles, as it contains second-order spatial derivatives of shape-functions.

Remark 4. The $\mathbf{G}_p^{\mathrm{el}}$ calculation leads to (for $n_{\mathrm{sd}} = 3$):

$$\mathbf{G}_p^{\mathrm{el}} = \mathbf{L}^{\mathrm{T}}\mathbf{1}\widetilde{\mathbf{N}} = \vec{\nabla}\widetilde{\mathbf{N}}. \tag{51}$$

3.2.1. Linearization of the residual part

Expressing the residual part of the stabilizing term at step $(n+1)$, iteration $(i+1)$:

$$\mathbf{L}^{\mathrm{T}}\boldsymbol{\sigma}_{n+1}^{i+1}(\mathbf{u}^h, p^h) + \mathbf{f} = \mathbf{L}^{\mathrm{T}}(\boldsymbol{\sigma}_{n+1}^{i} + \Delta\boldsymbol{\sigma}) + \mathbf{f} \overset{\text{def.}}{=} \mathbf{R}_{\sigma,n+1}^{i} + \Delta\mathbf{R}_{\sigma} + \mathbf{f}, \tag{52}$$

where the incremental constitutive equation (Eq. (30)) can be used in order to derive an expression for $\Delta\mathbf{R}_{\sigma}$:

$$\Delta\mathbf{R}_{\sigma} = \mathbf{L}^{\mathrm{T}}(\overline{\mathbf{D}}^{uu}\mathbf{B}\Delta\mathbf{u} + \overline{\mathbf{D}}^{up}\widetilde{\mathbf{N}}\Delta\mathbf{p}), \tag{53}$$

and therefore:

$$\mathbf{R}_{\sigma,n+1}^{i+1} = \mathbf{R}_{\sigma,n+1}^{i} + \mathbf{L}^{\mathrm{T}}\overline{\mathbf{D}}^{uu}\mathbf{B}\Delta\mathbf{u} + \mathbf{L}^{\mathrm{T}}\overline{\mathbf{D}}^{up}\widetilde{\mathbf{N}}\Delta\mathbf{p} \overset{\text{def.}}{=} \mathbf{R}_{\sigma,n+1}^{i} + \mathbf{G}_u^{\mathrm{ep}}\Delta\mathbf{u}_{n+1}^{i+1} + \mathbf{G}_p^{\mathrm{ep}}\Delta\mathbf{p}_{n+1}^{i+1}. \tag{54}$$

3.2.2. Back to the matrix form

Collecting weighting and residual parts of the stabilizing term leads to:

$$\sum_{e=1}^{n_{\mathrm{el}}} \int_{\Omega^e} (\mathbf{G}_u^{\mathrm{el}}\mathbf{w} + \mathbf{G}_p^{\mathrm{el}}\mathbf{q})^{\mathrm{T}}\boldsymbol{\tau}(\mathbf{R}_{\sigma,n+1}^{i} + \mathbf{G}_u^{\mathrm{ep}}\Delta\mathbf{u} + \mathbf{G}_p^{\mathrm{ep}}\Delta\mathbf{p} + \mathbf{f})\,\mathrm{d}\Omega. \tag{55}$$

Adding these terms to the matrix equation (45) we end up with the following system of equations:

$$\begin{bmatrix} \mathbf{K}_{uu} + \mathbf{K}'_{uu} & \mathbf{K}_{up} + \mathbf{K}'_{up} \\ -\mathbf{K}_{pu} + \mathbf{K}'_{pu} & -\mathbf{K}_{pp} + \mathbf{K}'_{pp} \end{bmatrix} \begin{Bmatrix} \Delta\mathbf{u} \\ \Delta\mathbf{p} \end{Bmatrix} = \begin{Bmatrix} \mathbf{F}_u + \mathbf{F}'_u \\ -\mathbf{F}_p + \mathbf{F}'_p \end{Bmatrix}, \tag{56}$$

where

$$\mathbf{K}'_{uu} = \sum_{e=1}^{n_{\mathrm{el}}} \int_{\Omega^e} \mathbf{G}_u^{\mathrm{el,T}}\boldsymbol{\tau}\mathbf{G}_u^{\mathrm{ep}}\,\mathrm{d}\Omega, \tag{57}$$

$$\mathbf{K}'_{up} = \sum_{e=1}^{n_{el}} \int_{\Omega^e} \mathbf{G}_u^{el,T} \boldsymbol{\tau} \mathbf{G}_p^{ep} \, d\Omega, \tag{58}$$

$$\mathbf{K}'_{pu} = \sum_{e=1}^{n_{el}} \int_{\Omega^e} \mathbf{G}_p^{el,T} \boldsymbol{\tau} \mathbf{G}_u^{ep} \, d\Omega, \tag{59}$$

$$\mathbf{K}'_{pp} = \sum_{e=1}^{n_{el}} \int_{\Omega^e} \mathbf{G}_p^{el,T} \boldsymbol{\tau} \mathbf{G}_p^{ep} \, d\Omega, \tag{60}$$

$$\mathbf{F}'_{u} = -\sum_{e=1}^{n_{el}} \int_{\Omega^e} \mathbf{G}_u^{el,T} \boldsymbol{\tau} (\mathbf{R}^i_{\sigma,n+1} + \mathbf{f}) \, d\Omega, \tag{61}$$

$$\mathbf{F}'_{p} = -\sum_{e=1}^{n_{el}} \int_{\Omega^e} \mathbf{G}_u^{el,T} \boldsymbol{\tau} (\mathbf{R}^i_{\sigma,n+1} + \mathbf{f}) \, d\Omega, \tag{62}$$

197 *3.2.3. Stabilization factor selection*

198 *3.2.3.1. Basic scalar form*. Dimensional analysis indicates the nature of τ. Dimension of $\int_\Omega w_i(\sigma_{ij,j} + f_i)\,d\Omega$ is
199 $[\frac{N}{m^2}]$. The same dimension holds for:

$$\sum_{e=1}^{n_{el}} \int_{\Omega} (\mathbb{L}(\mathbf{w}^h, q^h))^T \boldsymbol{\tau} (\mathscr{L}(\mathbf{u}^h, p^h) + \mathbf{f}) \, d\Omega, \tag{63}$$

201 where $\mathbb{L}$, $\mathscr{L}$ and $\mathbf{f}$ are $[\frac{N}{m^3}]$. Hence τ must be $[\frac{N}{m^3}] \cdot [\frac{m^3}{N}]^2 = [\frac{m^4}{N}]$ and we can conclude:

$$\text{Units}(\tau) = \left[\frac{m^2}{\frac{kN}{m^2}} \right]. \tag{64}$$

203 Similarly to what has been done in fluid mechanics, arguing that the equations that govern Stokes flow
204 are the same that govern incompressible elasticity, we define τ as being (see [10]):

$$\tau = \frac{\alpha^e (h^e)^2}{2\mu}, \tag{65}$$

206 α^e is a dimensionless scalar factor which has to be calibrated. h^e is a characteristic length of the element and
207 μ is the element's material shear modulus. The characteristic length of the element has some directional
208 character (consider for instance a thick cylinder test solved in the plane-strain format) and thus, following
209 the idea proposed by Oñate [13] we compute the element size as the largest projection of an element edge on
210 the direction of the increment of accumulated displacements, computed at the element center.
211 The scalar form of the stabilization operator $\boldsymbol{\tau}$ is the simplest choice. Deriving sophisticated formula
212 applicable to any elasto-plastic model and taking into account the element distortion does not seem to be
213 possible in general. Hereafter we exclusively consider the scalar form corresponding to elasticity with a
214 directional measure of the element size.

215 *3.3. An alternative: the Laplacian pressure operator scheme (LPOS)*

216 Following Brezzi and Pitkaranta [4] Pastor et al. [15] propose to add a different term to the original
217 mixed problem defined by Eq. (38). Instead of weighting the residual of the equilibrium equation, they

propose to add to the pressure equation the divergence of the equilibrium equation multiplied by a constant dependent on the mesh size which yields:

$$-\left(\varepsilon_{ii}^{e}-\frac{p}{K}\right)+\tau\nabla^{2}p=0, \tag{66}$$

The details of this derivation are given in Appendix B.

Remark 5. A negative sign is introduced in order to get a positive-definite system.

For τ, Pastor [15] uses the following definition, after Hughes et al. [10]:

$$\tau=\frac{\alpha^{e}(h^{e})^{2}}{2\mu}, \tag{67}$$

The incremental matrix system to be solved at each iteration therefore becomes:

$$\begin{bmatrix}\mathbf{K}_{uu} & \mathbf{K}_{up}\\ -\mathbf{K}_{pu} & -\mathbf{K}_{pp}+\mathbf{K}'_{pp}\end{bmatrix}\begin{Bmatrix}\mathbf{\Delta u}\\ \mathbf{\Delta p}\end{Bmatrix}=\begin{Bmatrix}\mathbf{F}_{u}\\ -\mathbf{F}_{p}+\mathbf{F}'_{p}\end{Bmatrix}, \tag{68}$$

where $\mathbf{K}_{uu}$, $\mathbf{K}_{up}$, $\mathbf{K}_{pu}$, $\mathbf{K}_{pp}$, $\mathbf{F}_{u}$ and $\mathbf{F}_{p}$ are given again by Eqs. (39)–(44) and:

$$\mathbf{K}'_{pp}=\sum_{e=1}^{n_{\mathrm{el}}}\int_{\Omega^{e}}(\vec{\nabla}\widetilde{\mathbf{N}})^{\mathrm{T}}\tau(\vec{\nabla}\widetilde{\mathbf{N}})\,\mathrm{d}\Omega, \tag{69}$$

$$\mathbf{F}'_{p}=-\sum_{e=1}^{n_{\mathrm{el}}}\int_{\Omega^{e}}(\vec{\nabla}\widetilde{\mathbf{N}})^{\mathrm{T}}\tau(\vec{\nabla}\widetilde{\mathbf{N}}\mathbf{p}^{i}_{n+1})\,\mathrm{d}\Omega. \tag{70}$$

4. Numerical examples

4.1. Example 1: incompressible elasticity analogy with the Stokes driven cavity flow

4.1.1. First analysis: bilinear quadrilaterals mesh

We apply first the unstabilized mixed formulation (Eq. (45)) to a nearly incompressible elasticity problem ($E=100\,000$ kN/m^2, $\nu=0.49999$) inspired by the Stokes driven cavity flow (see Figs. 1 and 2). Fig. 3 shows that the pressure field exhibits strong oscillations. Applying the stabilized GLS-A or GLS-B scheme, and gradually increasing the stabilization parameter α^{e} included in τ, the spurious oscillations in the pressure fields are eliminated (see Figs. 4 and 5). The observed optimal value of α^{e} is close to 0.5. If α^{e} is too small, oscillations remain in the pressure field, while if α^{e} is too large, stabilization will be too strong and the pressure field fails to capture the correct solution in the corners (see Fig. 6). Looking at the pressure distribution along a vertical line ($x/H=0.1$) and comparing the solutions with a reference solution given by the BBAR method (see Appendix C), Fig. 7 shows that $\alpha^{e}\cong 0.5$ yields a slight difference compared to the BBAR method. By comparing the pressure fields obtained for the two different stabilization schemes (GLS-A and GLS-B) (see Figs. 4 and 5) we may conclude that the addition of the $\mathbf{G}_{u}\mathbf{w}$ term in the weighting part of the GLS-A scheme does not have a significant influence on the solution. In all the considered examples the element size is computed as the square root of the element area and kept constant.

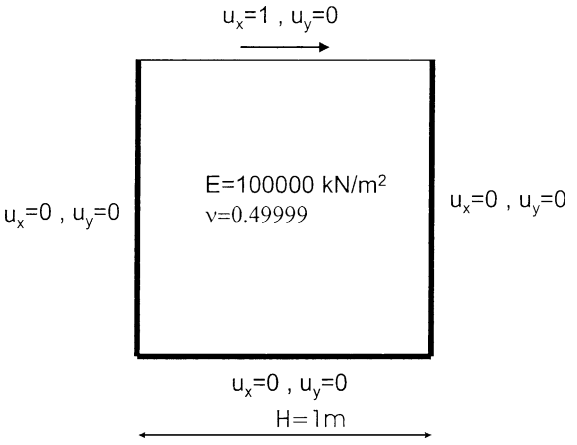

Fig. 1. Cavity flow analogy, geometry and properties.

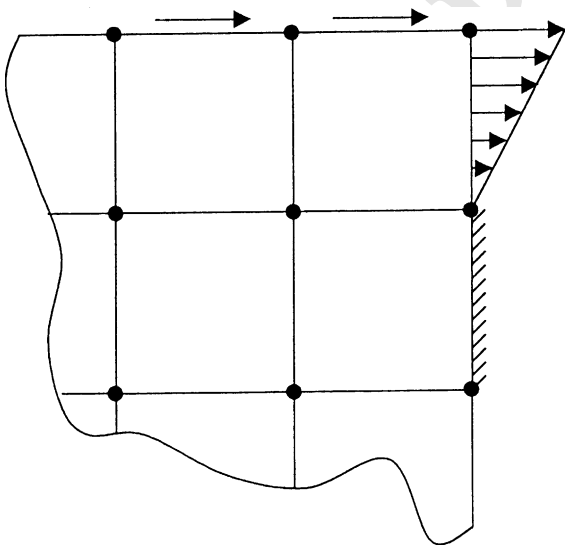

Fig. 2. Cavity flow analogy, corner boundary conditions.

Remark 6. Mesh-independence has been assessed by computing the same example with three different quadrilateral meshes (10×10, 20×20 and 40×40), keeping a stabilization parameter value of $\alpha^e = 0.5$. Pressure and displacement fields were correctly reproduced for these three cases.

4.1.2. Mixing different elements in the same mesh

Considering again example 1 with $\alpha^e = 0.5$ for quadrilateral elements and $\alpha^e = 0.25$ for triangles, (see Fig. 8), the stabilized solution (GLS-B) obtained when mixing bilinear quadrilaterals and linear triangles is shown not to suffer from oscillatory patterns, such as the mixture of BBAR quadrilaterals and linear triangles does (see Figs. 9 and 10). In the considered example the element size was computed as the square root of the element area and kept constant.

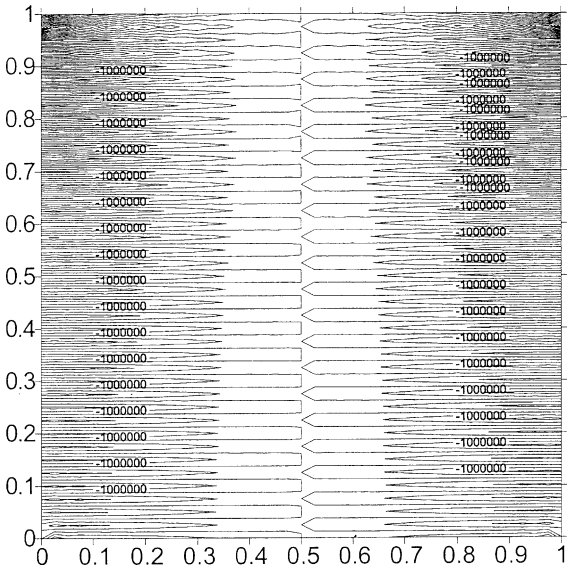

Fig. 3. Pressure elevations for $\alpha^e = 0.0$.

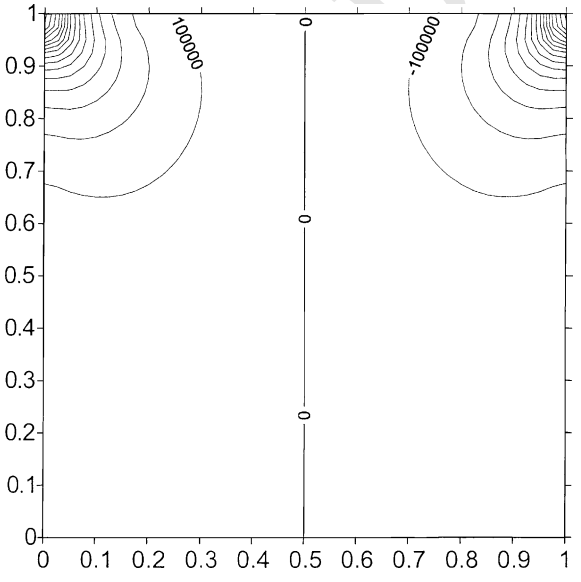

Fig. 4. Pressure elevations for $\alpha^e = 0.5$ (GLS-A).

255 *4.2. Example 2: elasto-plastic thick cylinder*

256 *4.2.1. Problem statement and analytical solution*

257 This test concerns a thick cylinder loaded by an internal pressure. The analytical solution is given in [9].
258 The internal and external radii of the cylinder are $a = 1.0$ and $b = 2.0$ m, and we denote by c the plastic
259 radius. Young modulus $E = 21\,000$ kN/m^2 and Poisson ratio $\nu = 0.49999$. The original solution [9] involves

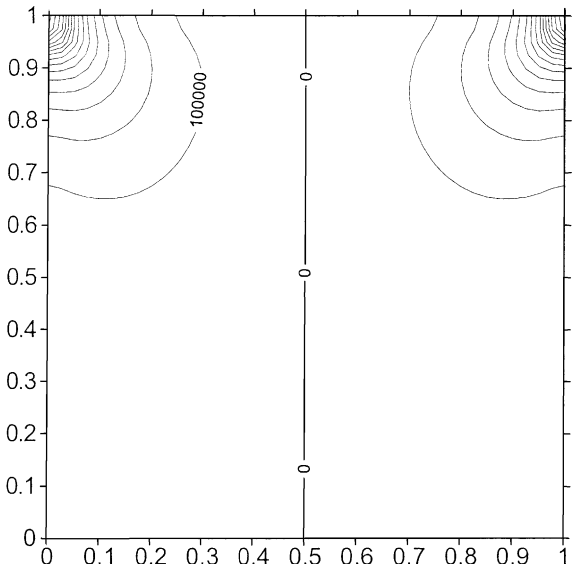

Fig. 5. Pressure elevations for $\alpha^e = 0.5$ (GLS-B).

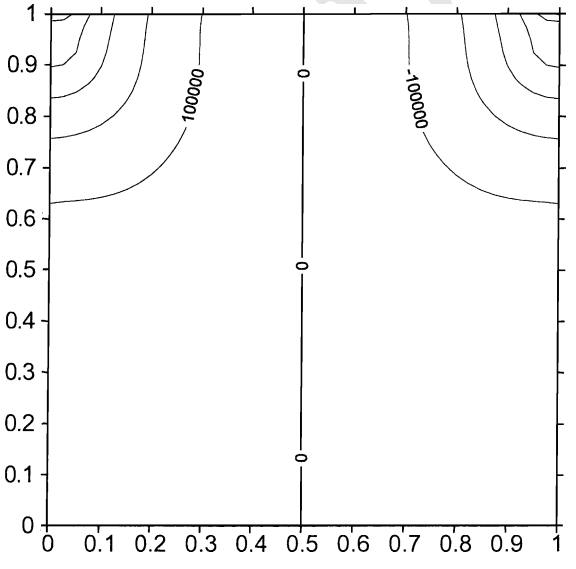

Fig. 6. Pressure elevations for $\alpha^e = 10.0$ (GLS-B).

Tresca's yield criterion: $\sigma_\theta - \sigma_r = \sigma_y = 24$ kN/m^2, where σ_θ is the circumferential stress, σ_r the radial stress and σ_y the yield stress (the longitudinal stress σ_z does not play any role in the plastic process as $v \to 0.5 \Rightarrow \sigma_z = \frac{1}{2}(\sigma_\theta + \sigma_r)$) (Fig. 11).

In the incompressible plane strain case, a von Mises criterion equivalent to the Tresca criterion (see [9] p. 117) can be expressed as: $\sigma_\theta - \sigma_r = \sigma_{y'} = \frac{2\sigma_y}{\sqrt{3}}$, which corresponds to a value of the von Mises parameter $k = \frac{\sigma_y}{\sqrt{3}} = 13.8564$ kN/m^2.

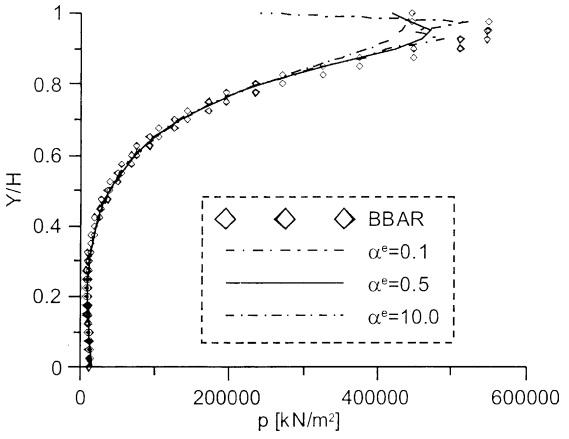

Fig. 7. Pressure elevations for $\alpha^e = 0.5$ (GLS-B).

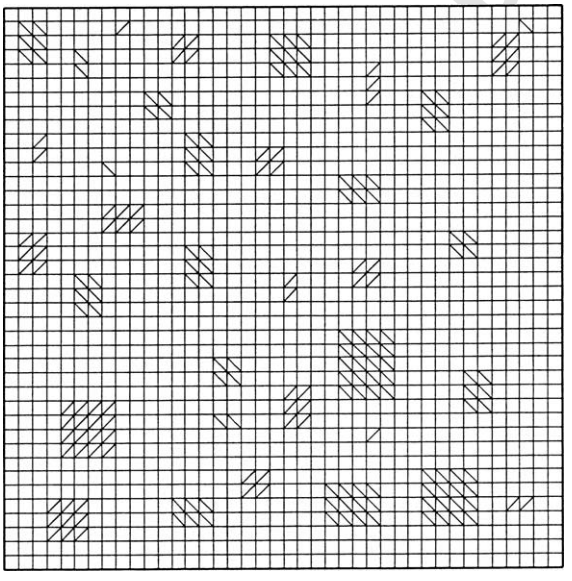

Fig. 8. Cavity flow analogy: Q4 + T3 mesh.

The internal pressure p is varied from 8 kN/m^2 (before yielding occurs) to 20 kN/m^2, the latter value corresponding to the total plastification of the cylinder.

The analytical solution for this test is given in the Appendix A.

4.2.2. h-Convergence study

The existence of an analytical solution for the thick cylinder test for the case of a nearly incompressible elasto-plastic material, makes it possible to define a procedure to find an "optimal" stabilization parameter α^e. We consider the meshes of one quarter of the cylinder (see Figs. 12 and 13). and we plot the normalized L_2^* pressure error norm (Eq. (71)) as a function of α^e for different internal pressures and hence stages of

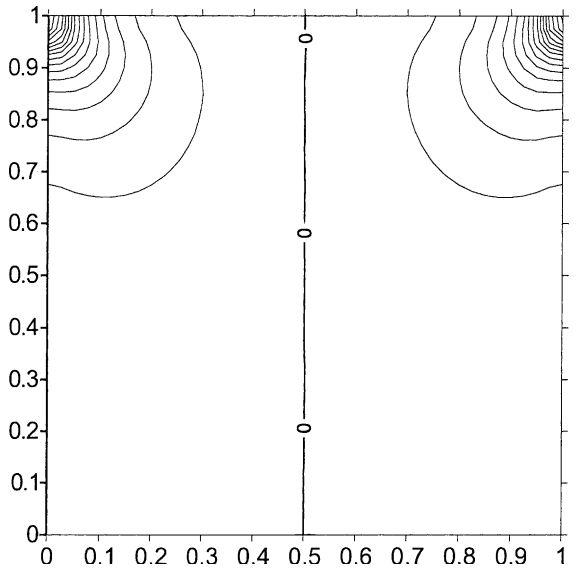

Fig. 9. Cavity flow analogy: pressure field for Q4+T3 (GLS-B scheme) solution.

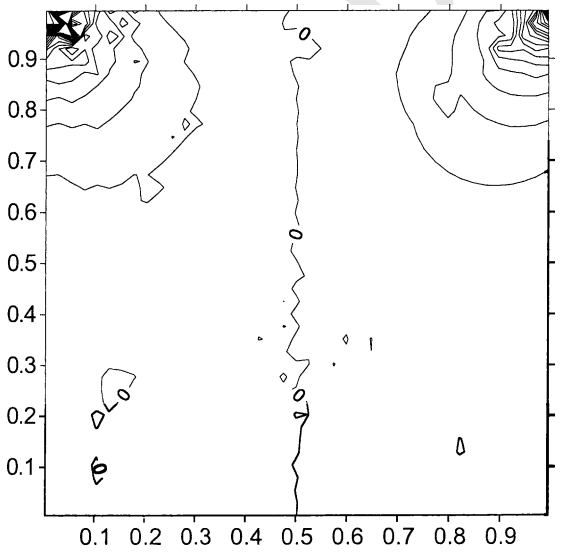

Fig. 10. Cavity flow analogy: pressure field for Q4-BBAR + T3 solution.

274 plastification; here, for $p = 10$ kN/m the cylinder remains elastic and for $p = 18$ kN/m it is plastified to
275 about 60%, meaning that the plastic radius $c \cong a + 0.6(b - a)$.

$$L_2^*(\phi) = \sqrt{\frac{\Sigma_{\text{el}} \int_{\Omega_e} (\phi^h - \phi)^{\mathrm{T}} (\phi^h - \phi)\, \mathrm{d}\Omega}{\Sigma_{\text{el}} \int_{\Omega_e} (\phi^{\mathrm{T}} \phi)\, \mathrm{d}\Omega}}. \tag{71}$$

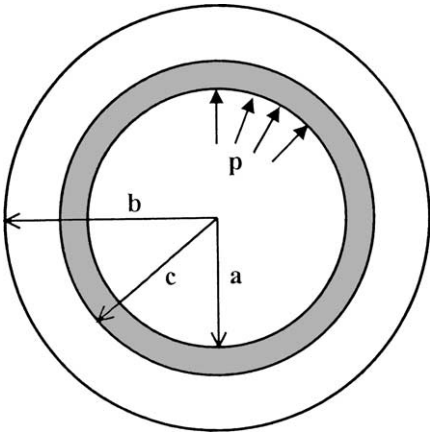

Fig. 11. Thick cylinder test geometry.

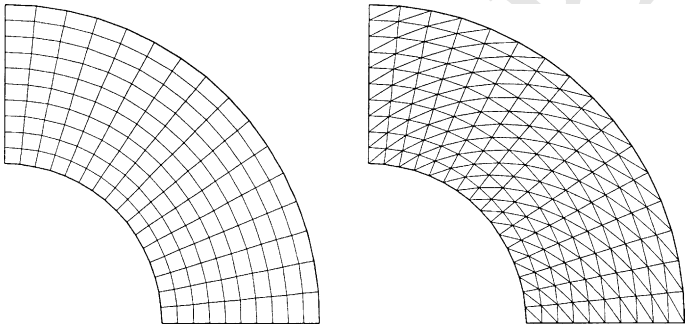

Fig. 12. Regular meshes with 10×16 rectangular elements pattern.

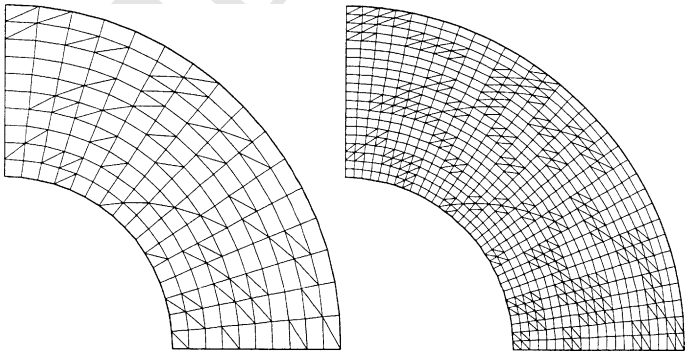

Fig. 13. Mixed meshes with 10×16 and 20×32 rectangular element patterns. Denser meshes are built on the same pattern.

277 Values of α^e which minimize the L_2^* pressure error appear to be in the range 0.25–0.50 for quadrilateral
278 elements (see Fig. 14) and between 0.10 and 0.50 for triangular elements (see Fig. 15), in the elasto-plastic
279 regime; this is confirmed by a convergence study based on the L_2^* displacement error (see Figs. 16 and 17).

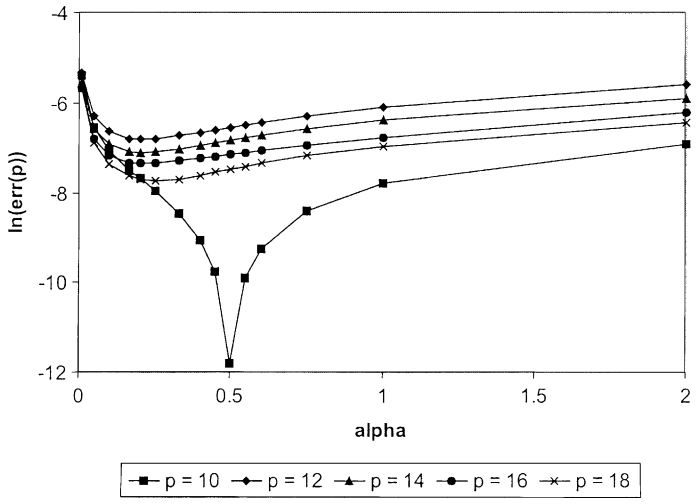

Fig. 14. L_2^* pressure error norm for Q4 elements (GLS-B formulation).

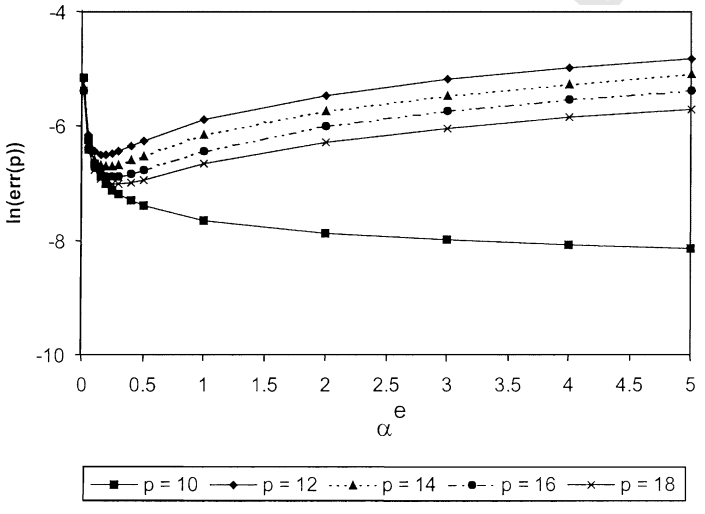

Fig. 15. L_2^* pressure error norm for T3 elements (GLS-B formulation).

Remark 7. Only results corresponding to the GLS-B formulation are shown here, but quasi identical results were obtained with GLS-A formulation and slightly different ones with LPOS.

Remark 8. The p pressure field is constant in the elastic case, resulting in a very low error minimum corresponding to $\alpha^e = 0.5$ for quadrilateral elements and $\alpha^e > 2$ for triangular elements.

Remark 9. In all simulations $h^e = \frac{b-a}{N}$, where N is the number of elements in the radial direction. This setting preserves a directional character of the stabilization factor τ.

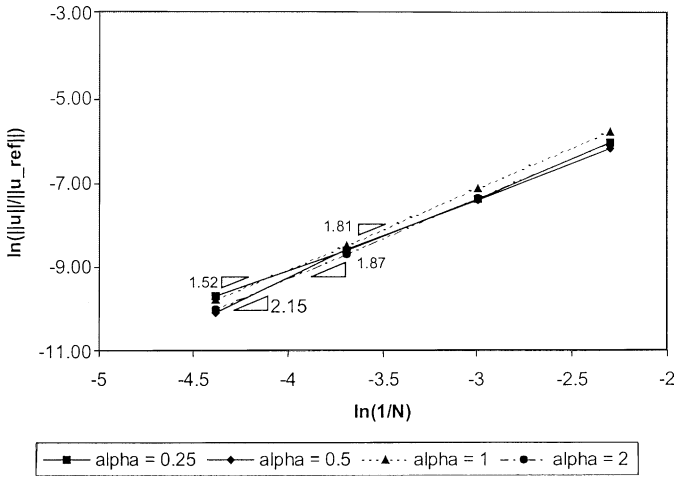

Fig. 16. Convergence study on L_2^* displacement error norm for Q4 elements (GLS-B formulation).

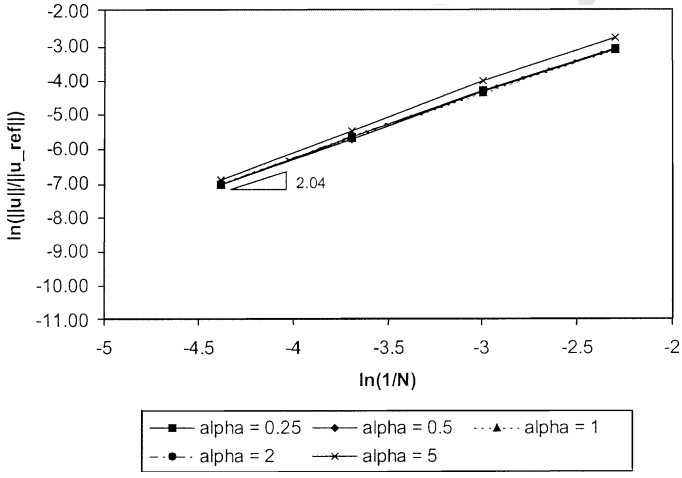

Fig. 17. Convergence study on L_2^* displacement error norm for T3 elements (GLS-B formulation).

4.2.2.1. Comparison of formulations. A convergence study for displacement and pressure errors is performed next on the same thick cylinder test problem, again for the nearly incompressible case. Stabilized formulations GLS-A, GLS-B and LPOS are examined. Meshes composed of $N = 10 \times 16$, $N = 20 \times 32$, $N = 40 \times 64$ and $N = 80 \times 128$ nodes using quadrilateral or triangular elements as well as quadrilateral and triangular elements mixtures (see Fig. 13), are considered. Linear displacement and pressure interpolations are used in all cases. Values of α^e adopted here are $\alpha^e = 0.50$ for quadrilateral elements and $\alpha^e = 0.25$ for triangular elements.

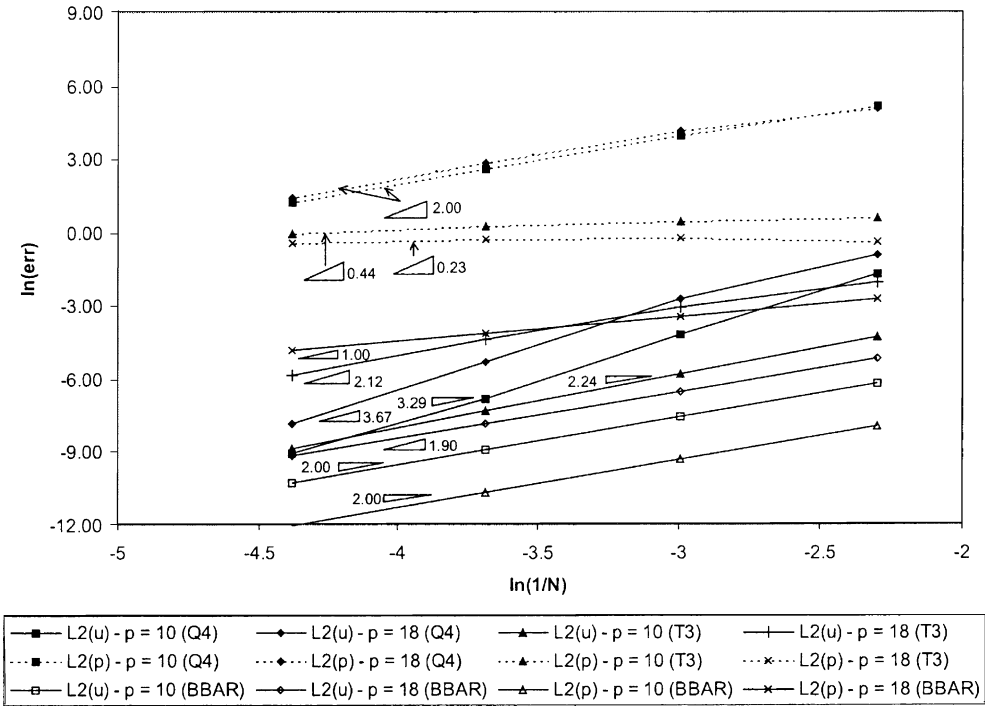

Fig. 18. L_2^* norms for standard u–p ($\alpha^e = 0.0$) and BBAR formulations.

Remark 10. Erratic convergence of standard u–p formulations (see Fig. 18) illustrates the effect of locking and pressure oscillations as compared to a BBAR formulation, which shows convergence of order 2 for displacement and pressure norms in elastic, regime and order 1 for p in elasto-plastic regime.

Remark 11. Fig. 19 shows that, on quads, convergence rates of Order 2 are observed for GLS-A, GLS-B, LPOS and BBAR formulations for displacements and for pressures in the elastic regime as well as for displacements in the elasto-plastic regime. In the elasto-plastic regime order 1.31 is observed for pressure in stabilized formulations, order 1 for BBAR (Table 2).

Remark 12. GLS-A, GLS-B and LPOS formulations perform in a similar manner. For triangles, GLS-A and GLS-B formulations coincide (Fig. 20). Observed pressure convergence rate in the elastic range is less for triangles (order 1.48 than for quads (order 2.0)), order 1.48, while in the plastic range triangles exhibit higher pressure convergence rate (1.50) than quads (1.31). However, the pressure error magnitude is always lower for quads than for triangles (see Table 1).

Remark 13. Mixing triangles and quads leads to a degradation of the convergence rates, which tends however to alleviate as the mesh is refined (see Fig. 21).

Convergence tests on distorted meshes are presented next (Figs. 22–27). Only results obtained with the GLS-B formulation are presented. Mesh distortion is achieved by a random perturbation of both nodal coordinates, of amplitude $0.1 \times h$ up to $0.2 \times h$, where h is the reference element size of the regular mesh measured in the radial direction. As an intuitive distortion correction the element size which appears in the

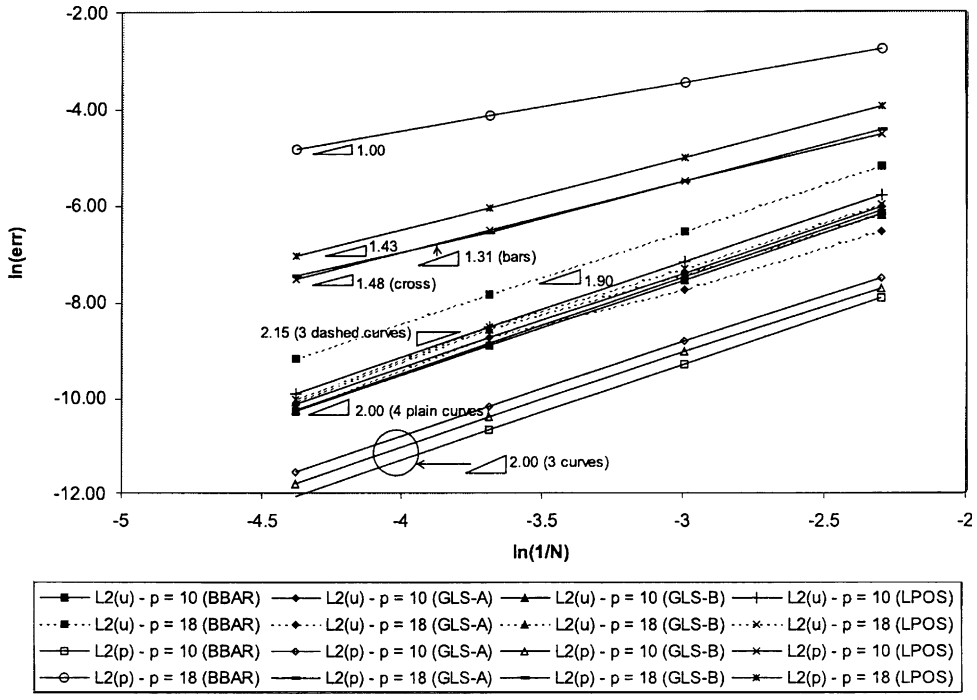

Fig. 19. L_2^* norms for stabilized Q4 elements ($\alpha^e = 0.5$).

Table 1
Convergence rates for undistorted meshes

	L_2^*	$p = 10$ kN/m^2 (elastic)		$p = 18$ kN/m^2 (elasto-plastic)	
		Rate	Order of magnitude[a]	Rate	Order of magnitude[a]
Q4-BBAR	u	2.00	−10.31	1.90	−9.19
Q4-BBAR	p	2.00	−12.06	1.00	−4.84
Q4-GLS-B	u	2.00	−10.26	2.15	−10.09
Q4-GLS-B	p	2.00	−11.80	1.31	−7.47
T3-GLS-B	u	2.00	−9.21	2.04	−7.09
T3-GLS-B	p	1.48	−7.11	1.50	−7.02
Q4+T3-GLS-B	u	2.01	−9.72	1.41	−8.47
Q4+T3-GLS-B	p	1.29	−7.21	1.33	−6.85

[a] Of relative error for most refined mesh according to Eq. (71).

311 stabilization factor is taken here as the largest projection of an element edge on the vector of accumulated
312 displacements (in the considered case it practically coincides with the radial direction).

313 **Remark 14.** In the elastic regime the displacement convergence rate for stabilized T3 and Q4 elements is of
314 order 2.0 (see Figs. 22, 24 and 26. Stabilized Q-4 elements exhibit lower magnitude of the error in the L_2^*
315 norm (see also Tables 3 and 4).

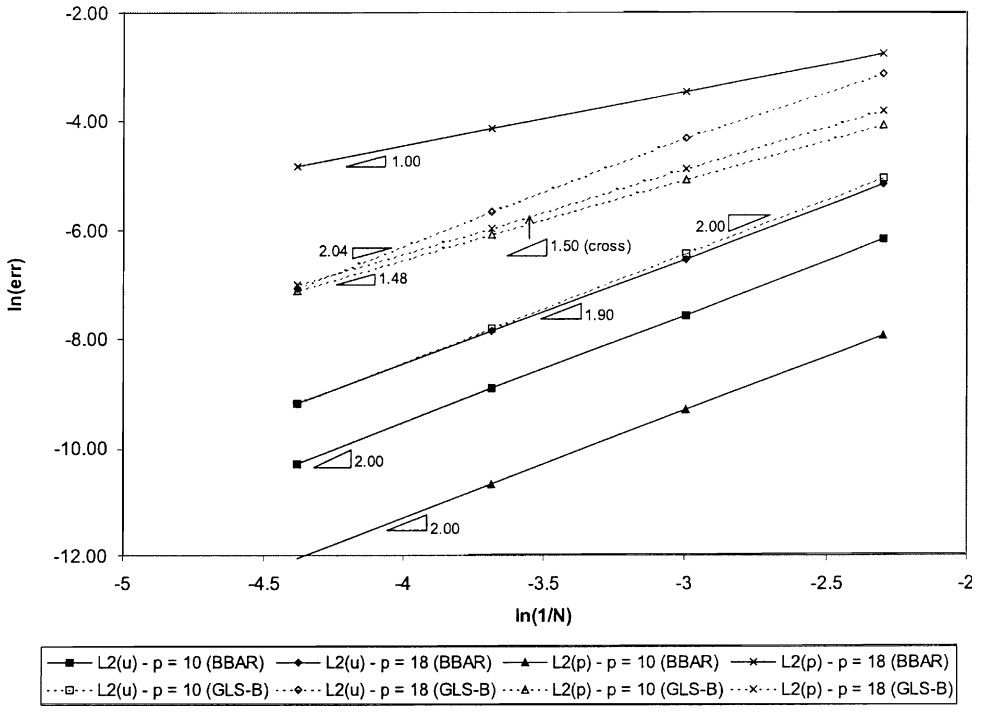

Fig. 20. L_2^* norms for stabilized T3 elements ($\alpha^e = 0.25$), comparison with BBAR on quads.

Table 2
Convergence rates for distorted BEAR elements

	Distortion	L_2^*	$p = 10$ kN/m^2		$p = 18$ kN/m^2	
			Rate	Order of magnitude	Rate	Order of magnitude
Q4-BBAR	$0.10h^e$	u	1.94	−10.11	1.95	−9.15
Q4-BBAR	$0.10h^e$	p	0.39	−3.90	0.84	−4.28
Q4-BBAR	$0.15h^e$	u	1.92	−9.92	2.07	−9.09
Q4-BBAR	$0.15h^e$	p	0.54	−3.87	0.87	−4.22
Q4-BBAR	$0.20h^e$	u	1.92	−9.73	2.21	−9.02
Q4-BBAR	$0.20h^e$	p	0.65	−3.84	0.90	−4.19

Remark 15. In the elasto-plastic regime the displacement convergence rate for stabilized Q4 elements decreases with the distortion ratio and is definitely smaller than 2.00. This effect is not observed for T3 stabilized elements (see Figs. 23, 25 and 27 and Tables 3 and 4). However stabilized Q-4 elements again exhibit lower magnitude of the error in the L_2^* norm.

Remark 16. In the elastic regime the pressure convergence rate for stabilized Q4 elements degrades from 2.00 to 0.98 when distortion is present (see Figs. 22, 24 and 26) but is insensitive to the rate of the element distortion. The pressure convergence rate for T3 stabilized elements drops from 1.29 to 1.16 when distortion is present and is slightly sensitive to the rate of the element distortion but the magnitude of the error is always smaller than for Q4 elements.

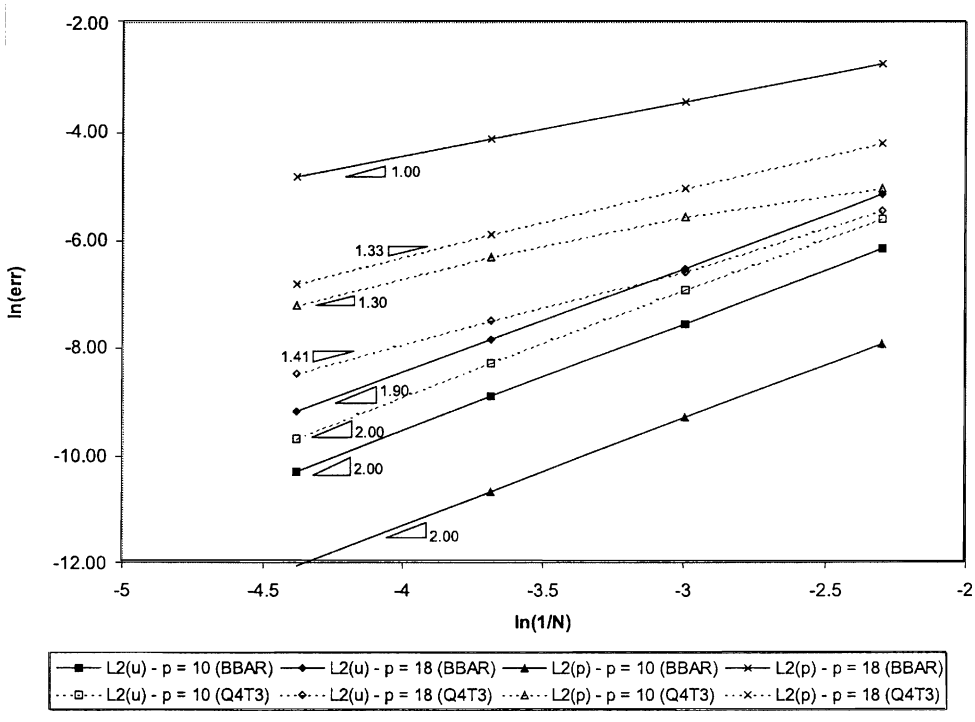

Fig. 21. L_2^* norms for stabilized Q4 and T3 elements (GLS-B) (mixed meshes).

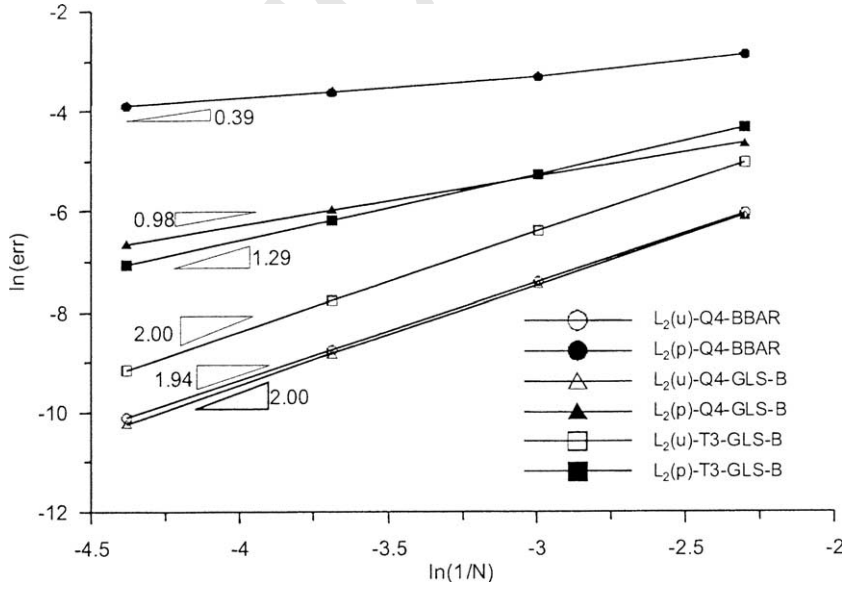

Fig. 22. L_2^* norms for stabilized Q4 and T3 elements (GLS-B formulation) (distortion $0.15 \times h$) ($p = 10$ kN/m^2).

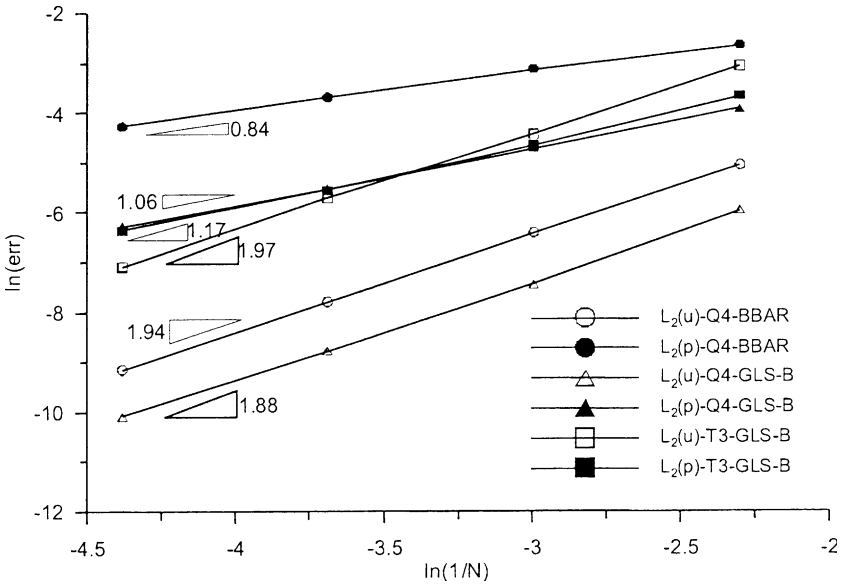

Fig. 23. L_2^* norms for stabilized Q4 and T3 elements (GLS-B formulation) (distortion $0.15 \times h$) ($p = 18$ kN/m^2).

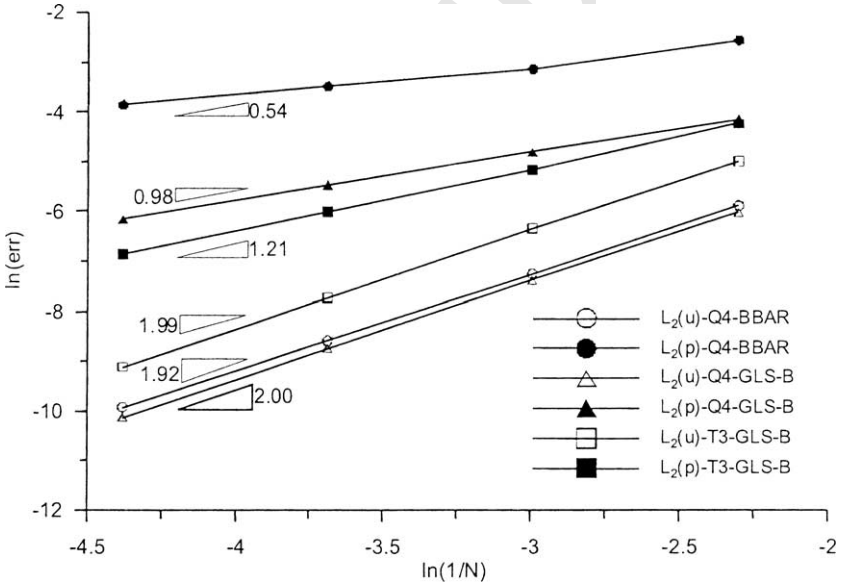

Fig. 24. L_2^* norms for stabilized Q4 and T3 elements (GLS-B formulation) (distortion $0.1 \times h$) ($p = 10$ kN/m^2).

Remark 17. In the elastic–plastic regime the pressure convergence rates for stabilized Q4 and T3 elements are again lower then for undistorted meshes and decrease with the distortion ratio (see Figs. 23, 25 and 27). The magnitude of the pressure error generated by T3 stabilized elements is smaller than for Q4 elements for any distortion ratios from range 0.10–0.20.

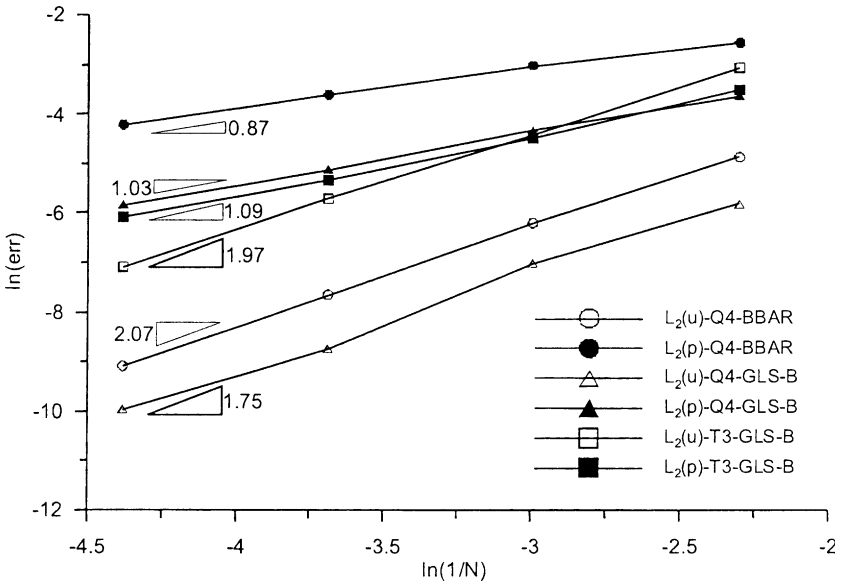

Fig. 25. L_2^* norms for stabilized Q4 and T3 elements (GLS-B formulation) (distortion $0.1 \times h$) ($p = 18$ kN/m^2).

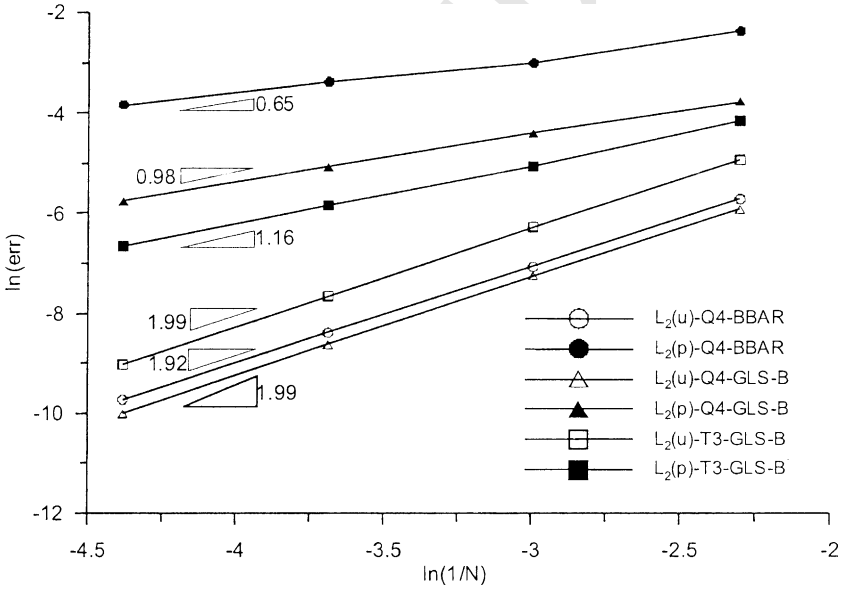

Fig. 26. L_2^* norms for stabilized Q4 and T3 elements (GLS-B formulation) (distortion $0.2 \times h$) ($p = 10$ kN/m^2).

Remark 18. The GLS-A formulation fails to converge in the elastic–plastic regime for distortion ratio higher than 0.15.

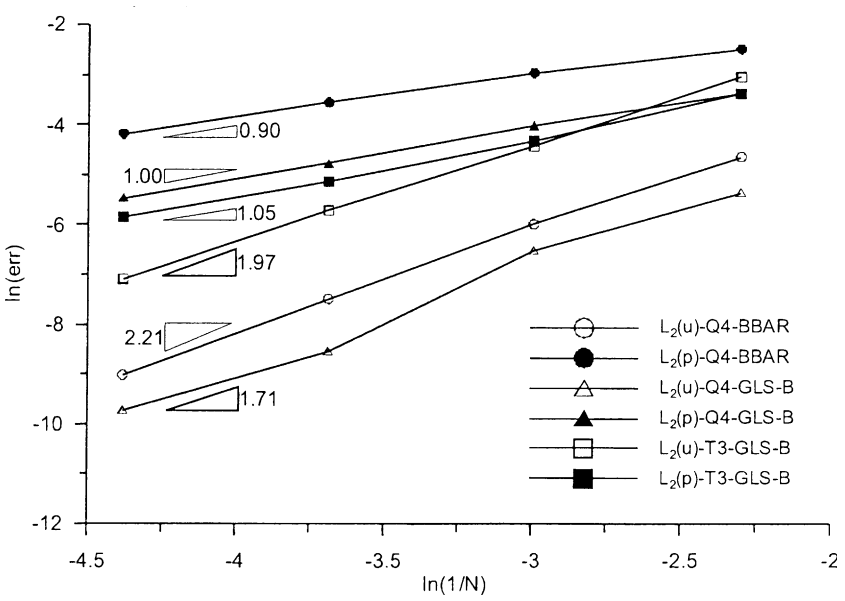

Fig. 27. L_2^* norms for stabilized Q4 and T3 elements (GLS-B formulation) (distortion $0.2 \times h$) ($p = 18$ kN/m^2).

Table 3
Convergence rates for distorted Q4-GLS-B elements

	Distortion	L_2^*	$p = 10$ kN/m^2		$p = 18$ kN/m^2	
			Rate	Order of magnitude	Rate	Order of magnitude
Q4-GLS-B	$0.10h^e$	u	2.00	−10.22	1.88	−10.09
Q4-GLS-B	$0.10h^e$	p	0.98	−6.66	1.06	−6.27
Q4-GLS-B	$0.15h^e$	u	2.00	−10.13	1.75	−9.96
Q4-GLS-B	$0.15h^e$	p	0.98	−6.16	1.03	−5.84
Q4-GLS-B	$0.20h^e$	u	1.99	−10.01	1.71	−9.73
Q4-GLS-B	$0.20h^e$	p	0.98	−5.76	1.00	−5.46

Table 4
Convergence rates for distorted T3-GLS-B elements

	Distortion	L_2^*	$p = 10$ kN/m^2		$p = 18$ kN/m^2	
			Rate	Order of magnitude	Rate	Order of magnitude
T3-GLS-B	$0.10h^e$	u	2.00	−9.16	1.97	−7.09
T3-GLS-B	$0.10h^e$	p	1.29	−7.08	1.17	−6.37
T3-GLS-B	$0.15h^e$	u	1.99	−9.11	1.97	−7.09
T3-GLS-B	$0.15h^e$	p	1.21	−6.86	1.09	−6.08
T3-GLS-B	$0.20h^e$	u	1.99	−9.03	1.97	−7.09
T3-GLS-B	$0.20h^e$	p	1.16	−6.66	1.05	−5.85

5. Conclusion

This paper discusses stabilized finite element formulations in nearly incompressible elasticity and elasto-plasticity with applications in the field of continuum mechanics. Following the methodology used with

success in computational fluid dynamics, a stable mixed finite element scheme is derived by adding appropriate terms to the original matrix form of the problem. The need for such a formulation results from the fact that, to our knowledge, none of the methods available in the literature today is able to handle, within a single formulation, elasto-plasticity (in the presence of incompressible or dilatant plastic flow) on an unstructured mesh composed of (bi-)linear triangular and quadrilateral elements.

The first scheme that is discussed is the Galerkin/least-squares formulation (proposed for CFD by Franca [8] and Hughes et al. [12]). In this scheme, stabilizing terms are derived from a least-squares potential, and consistency is preserved as the residual of the governing equilibrium equation is explicitly present in these terms. We then show that neglecting the displacement term in the weighting part of the stabilizing terms—therefore keeping only the gradient of the pressure and getting a modified-GLS (GLS-B) scheme form-like to the SUPG method [2]—does not affect results and simplifies the linearization process in the elasto-plastic case.

The definition of the stabilization factor τ, an important aspect of stabilized formulations, is discussed, and a form of τ obtained by analogy with to the one proposed for Stokes flow stabilization in [10] is adopted.

The Laplacian pressure operator scheme (introduced for soil plasticity by Pastor et al. [15]) is also discussed, and shown to produce comparable results.

Typical benchmarks, namely a Stokes driven cavity flow analogy in incompressible elasticity and an elasto-plastic thick cylinder loaded by an internal pressure, demonstrate the validity of the proposed approach and are used to calibrate the stabilization factor τ. Although only nearly incompressible behavior is examined in this paper, the stabilized approach also applies to dilatant situations. Comparisons with the finite increment approach (FIC), advocated in [14], extensions to dilatant elasto-plasticity and applications in geomechanics will be addressed in companion papers [6,7].

6. Uncited references

[1,3,17,20]

Acknowledgements

The authors thank T.J.R. Hughes (University of Texas at Austin) for useful discussions at various stages of the research project and for inviting S. Commend to join his team at Stanford for a one year period during this research work, and T. Tezduyar (Rice University) for constructive suggestions at the early stage of the project. The financial support of the Fund of the 15th Congress of the Swiss National Committee on Large Dams and of the Swiss National Science Foundation under grant 21-49404.96 for the first author is gratefully acknowledged.

Appendix A. Elasto-plastic thick cylinder analytical solution

In the elastic regime, the radial displacement is given by:

$$u_{\mathrm{el}} = \frac{(1+\nu)p}{E\left(\frac{b^2}{a^2}-1\right)}\left[(1-2\nu)r + \frac{b^2}{r}\right], \tag{A.1}$$

where r is the radius at which the unknown value is computed. The radial and circumferential stresses read:

$$\sigma_r = \frac{-p\left(\frac{b^2}{r^2} - 1\right)}{\left(\frac{b^2}{a^2} - 1\right)}, \tag{A.2}$$

$$\sigma_\theta = \frac{p\left(\frac{b^2}{r^2} + 1\right)}{\left(\frac{b^2}{a^2} - 1\right)}. \tag{A.3}$$

For the partly plastic cylinder, the plastic radius c can be deduced from the following expression:

$$p = 2k\left[\ln\left(\frac{c}{a}\right) + \frac{1}{2}\left(1 - \frac{c^2}{b^2}\right)\right]. \tag{A.4}$$

The value of c can then be used to compute the new radial displacement after partial plastification of the cylinder:

$$u_{pl} = \frac{(1+v)kc^2}{Eb^2}\left[(1-2v)r + \frac{b^2}{r}\right], \tag{A.5}$$

and the stresses in the elastic region ($c < r < b$) now read:

$$\sigma_r = \frac{-kc^2\left(\frac{b^2}{r^2} - 1\right)}{b^2}, \tag{A.6}$$

$$\sigma_\theta = \frac{kc^2\left(\frac{b^2}{r^2} + 1\right)}{b^2}, \tag{A.7}$$

while the stresses in the plastic region ($a < r < c$) are given by:

$$\sigma_r = 2k\left(-\frac{1}{2} - \ln\left(\frac{c}{r}\right) + \frac{c^2}{2b^2}\right), \tag{A.8}$$

$$\sigma_\theta = 2k\left(\frac{1}{2} - \ln\left(\frac{c}{r}\right) + \frac{c^2}{2b^2}\right). \tag{A.9}$$

Appendix B. Derivation of the LPOS stabilization term

Taking the divergence of the equilibrium equation leads to:

$$\mathrm{div}(\sigma_{ij,j} + f_i) = 0. \tag{B.1}$$

Assuming that body forces are divergence-free and expressing $\sigma_{ij} = s_{ij} + \delta_{ij}p$:

$$\mathrm{div}(s_{ij,j} + p_{,i}) = 0, \tag{B.2}$$

or, introducing the Laplacian operator:

$$\mathrm{div}(s_{ij,j}) + \nabla^2 p = 0. \tag{B.3}$$

Introducing the continuity equation (9) into the computation of $\mathrm{div}(s_{ij,j})$ leads to, after some algebra [15]:

$$\mathrm{div}(s_{ij,j}) = \frac{4\mu}{3}\nabla^2\left(\frac{p}{K}\right). \tag{B.4}$$

Combining Eqs. (B.3) and (B.4) allows us to write:

$$\operatorname{div}(s_{ij,j}) + \nabla^2 p = \frac{\lambda + 2\mu}{K} \nabla^2 p = 0, \tag{B.5}$$

where $K = \lambda + \frac{2}{3}\mu$. The divergence of the equilibrium equation therefore reduces to $\nabla^2 p = 0$, and the stabilized pressure equation becomes:

$$-\left(\varepsilon^e_{ii} - \frac{p}{K}\right) + \tau \nabla^2 p = 0. \tag{B.6}$$

Appendix C. Modified BBAR method for plane-strain

The standard BBAR method, in plane-strain, satisfies the $\varepsilon_z = 0$ condition only in the weak sense. To recover its exact satisfaction at any point within the element, the BBAR method can be constructed by replacing $\mathbf{B}_i^{\text{vol}}$ matrix by a $\mathbf{B}_i^{\text{mean2D}}$ matrix

$$\mathbf{B}_i^{\text{mean2D}} = \begin{bmatrix} \frac{1}{2}N_{i,x} & \frac{1}{2}N_{i,y} \\ \frac{1}{2}N_{i,x} & \frac{1}{2}N_{i,y} \\ 0 & 0 \\ 0 & 0 \end{bmatrix}, \tag{C.1}$$

which corresponds to use a "modified" mean strain $\varepsilon^*_m = \frac{1}{2}(\varepsilon_x + \varepsilon_y)$ instead of standard mean strain $\varepsilon_m = \frac{1}{3}(\varepsilon_x + \varepsilon_y + \varepsilon_z)$ as in the original approach [11]. The differences between standard and modified plane-strain BBAR methods, and major advantages of the latter one, are discussed in [19].

References

[1] I. Babuška, Error bounds for finite element method, Num. Math. 16 (1971) 322–333.
[2] A.N. Brooks, T.J.R. Hughes, Streamline upwind/Petrov–Galerkin formulations for convection dominated flows with particular emphasis on the incompressible Navier–Stokes equations, Comput. Methods Appl. Mech. Engrg. 32 (1982) 199–259.
[3] F. Brezzi, On the existence, uniqueness and approximation of saddle-point problems arising from Lagrange multipliers, Revue Fr. d'Automatique Inf. Rech. Opér., Série Rouge Analyse Numérique R-2 8 (1974) 129–151.
[4] F. Brezzi, J. Pitkaranta, On the stabilization of finite element approximations of the Stokes problem, in: Efficient Solutions of Elliptic Problems, Notes on Numerical Fluid Mechanics, vol. 10, Vieweg-Wiesbaden, 1984, pp. 11–19.
[5] S. Commend, Stabilized finite elements in geomechanics, Swiss Federal Institute of Technology (EPFL) Ph.D. Dissertation #2391, 2001.
[6] S. Commend, A. Truty, Th. Zimmermann, Stabilized finite elements applied to elasto-plasticity: II. A comparison of formulations, in press.
[7] S. Commend, A. Truty, Th. Zimmermann, Stabilized finite elements for geomechanical applications, in press.
[8] L.P. Franca, New mixed finite element methods, Stanford University, Ph.D. Dissertation, 1987.
[9] R. Hill, The Mathematical Theory of Plasticity, Oxford Science Publications, 1950.
[10] T.J.R. Hughes, L.P. Franca, M. Balestra, A new finite element formulation for computational fluid dynamics: V. Circumventing the Babuska–Brezzi condition: a stable Petrov–Galerkin formulation of the Stokes problem accommodating equal-order interpolations, Comput. Methods Appl. Mech. Engrg. 59 (1986) 85–99.
[11] T.J.R. Hughes, The Finite Element Method: Linear Static and Dynamic Finite Element Analysis, Prentice-Hall, 1987.
[12] T.J.R. Hughes, L.R. Franca, G.M. Hulbert, A new finite element formulation for computational fluid dynamics: VIII. The Galerkin/least-squares method for advective–diffusive equations, Comput. Methods Appl. Mech. Engrg. 73 (1989) 173–189.
[13] E. Oñate, Derivation of stabilized equations for numerical solution of advective–diffusive transport and fluid flow problems, Comput. Methods Appl. Mech. Engrg. 151 (1998) 233–265.
[14] E. Oñate, A stabilized finite element method for incompressible viscous flows using a finite increment calculus formulation, Comput. Methods Appl. Mech. Engrg. 182 (2000) 355–370.

[15] M. Pastor, M. Quecedo, O.C. Zienkiewicz, A mixed displacement–pressure formulation for numerical analysis of plastic failure, Comput. Struct. 62-1 (1997) 13–23.
[16] J.C. Simo, M.S. Rifai, A class of mixed assumed strain methods and the method of incompatible modes, Int. J. Num. Methods Engrg. 29 (1990) 1595–1638.
[17] C.A. Taylor, T.J.R. Hughes, C.K. Zarins, Finite element modeling of blood flow in arteries, Comput. Methods Appl. Mech. Engrg. 158 (1998) 155–196.
[18] A. Truty, A Galerkin/least-squares finite element formulation for consolidation, Int. J. Num. Methods Engrg. 52 (2001) 763–786.
[19] A. Truty, On certain classes of mixed and stabilized mixed finite element formulations for single and two-phase geomaterials, Habilitation thesis 48, Cracow University of Technology, ISSN 0137-1363, 2002.
[20] O.C. Zienkiewicz, M. Huang, M. Pastor, Localization problems in plasticity using finite elements with adaptative remeshing, Int. J. Num. Anal. Methods Geomech. 19 (1995) 127–148.
[21] O.C. Zienkiewicz, R.L. Taylor, The Finite Element Method, vol. 1, The Basis, Butterworth & Heinemann, 2000.